Three-Dimensional Solution Structure of the Oxidized High Potential Iron−Sulfur Protein from *Chromatium vinosum* through NMR. Comparative Analysis with the Solution Structure of the Reduced Species†

Ivano Bertini,*,‡ Alexander Dikiy,‡ Dieter H. W. Kastrau,‡ Claudio Luchinat,§ and Pornthep Sompornpisut‡

Department of Chemistry, University of Florence, Via Gino Capponi 7, 50121 Florence, Italy, and the Institute of Agricultural Chemistry, University of Bologna, Viale Berti Pichat 10, 40127, Bologna, Italy

Received March 21, 1995; Revised Manuscript Received May 15, 1995®

ABSTRACT: The NMR solution structure of the oxidized HiPIP from *Chromatium vinosum* has been solved. Despite the fact that the protein is paramagnetic, 85% of the ^{1}H and 80% of the ^{15}N signals have been assigned. Through 1537 NOEs, out of which 1142 were found to be relevant for the structure determination, a family of structures has been obtained by distance geometry calculations. These structures have then been subjected to restrained energy minimization (REM) and restrained molecular dynamics (RMD) calculations in vacuum. Finally, the mean structure of the RMD family has been treated through RMD in water. The RMSD values for the backbone and heavy atoms within the RMD family are 0.57 ± 0.14 and 1.08 ± 0.16 Å, respectively. These values together with other parameters indicate that the structure is of good quality and as good as the structure of the reduced protein. The RMDw structures of the reduced and oxidized proteins are different beyond the experimental indetermination. The set of constraints for the reduced and oxidized forms have been used to treat the available X-ray structure by RMD in water. The two structures generated in this way are quite similar to their respective solution structures, thus confirming that the experimental constraints are capable of yielding two different structures from the same starting structural model. This is the first time that independently determined solution structures of two redox states of a paramagnetic protein are available. Differences between them and the X-ray structure are discussed.

NMR[1] of paramagnetic biomolecules in solution has developed later with respect to diamagnetic molecules because unpaired electrons broaden the ^{1}H lines, and connectivities become hard to detect (Bertini & Luchinat, 1986; Banci et al., 1991; Luchinat & Ciurli, 1993; La Mar, 1995). Pochapsky et al. (1994) succeeded in solving an NMR structure in solution of an oxidized Fe_2S_2 protein constituted by 106 amino acids, which has short nuclear T_1 values (≈1 ms) around the iron(III) ions. As a consequence of the large paramagnetism, the RMSD is relatively large and there is little information around the dimetallic center.

We succeeded in determining the solution structures of two reduced HiPIPs from *Ectothiorhodospira halophila* (Banci et al.1994) and *Chromatium vinosum* (Banci et al., 1995). They contain an Fe_4S_4 polymetallic center, with a paramagnetism at room temperature equivalent to $^1/_2$ electron per iron (Phillips et al., 1974). The T_1 values of the β-CH_2 cysteine protons are of the order of few milliseconds (2−7 ms) (Bertini et al., 1991). The molecular masses of these proteins are approximately 8 kDa (73 amino acids) (Breiter et al., 1991) and 9.5 kDa (85 amino acids) (Dus et al., 1967), respectively. The solution structures are comparable in quality to solution structures of diamagnetic proteins in absence of ^{13}C enrichment (Clore & Gronenborn, 1994). The RMSD of the backbone atoms are 0.51 and 0.62 Å, respectively. We have then attempted the determination of the solution structures of the oxidized proteins, which have a paramagnetism of 1.8 electrons per iron (Moss et al., 1969).

Here we report the solution structure of the oxidized HiPIP from *C. vinosum.* The structure is analogous to the structure of the reduced protein and allows us to discuss how the two structures are different beyond the experimental indetermination.

EXPERIMENTAL PROCEDURES

All chemicals used were of the best quality available. Native and ^{15}N enriched HiPIP from *C. vinosum* were prepared and purified in reduced form as described earlier (Bartsch, 1978). Oxidation of the protein was achieved by addition of solid $K_3[Fe(CN)_6]$ to the protein solution.

Samples for NMR spectroscopy (3 mM native protein and 1.5 mM ^{15}N labeled protein) were prepared in 50 mM phosphate buffer (either in H_2O or D_2O), pH 5.1. 1D and 2D homo- and heteronuclear NMR experiments were performed on a Bruker AMX spectrometer operating at 600.14 MHz proton Larmor frequency in a fashion analogous to that of the reduced protein (Banci et al., 1995).

For the structure calculation, volumes of assigned NOESY cross peaks were handled following the procedure described for the reduced protein (Banci et al., 1995), including

† This work is partially supported by "Progetto Finalizzato Biotecnologie", Comitato Biotechnologie e Biologia Molecolare, and "Comitato Scienze Agrarie" of CNR, Italy.

* Author to whom correspondence should be addressed. Phone: (39) 55-275-7549. Fax: (39) 55-275-7555.

‡ University of Florence.

§ University of Bologna.

® Abstract published in *Advance ACS Abstracts,* June 15, 1995.

[1] Abbreviations: NMR, nuclear magnetic resonance; 1, 2D, one, two dimensional; NOE, nuclear Overhauser effect; NOESY, nuclear Overhauser effect spectroscopy; TOCSY, total correlation spectroscopy; HMQC, heteronuclear multiple quantum correlation spectroscopy; DG, distance geometry, REM, restrained energy minimization, RMD, restrained molecular dynamics.

0006-2960/95/0434-9851$09.00/0

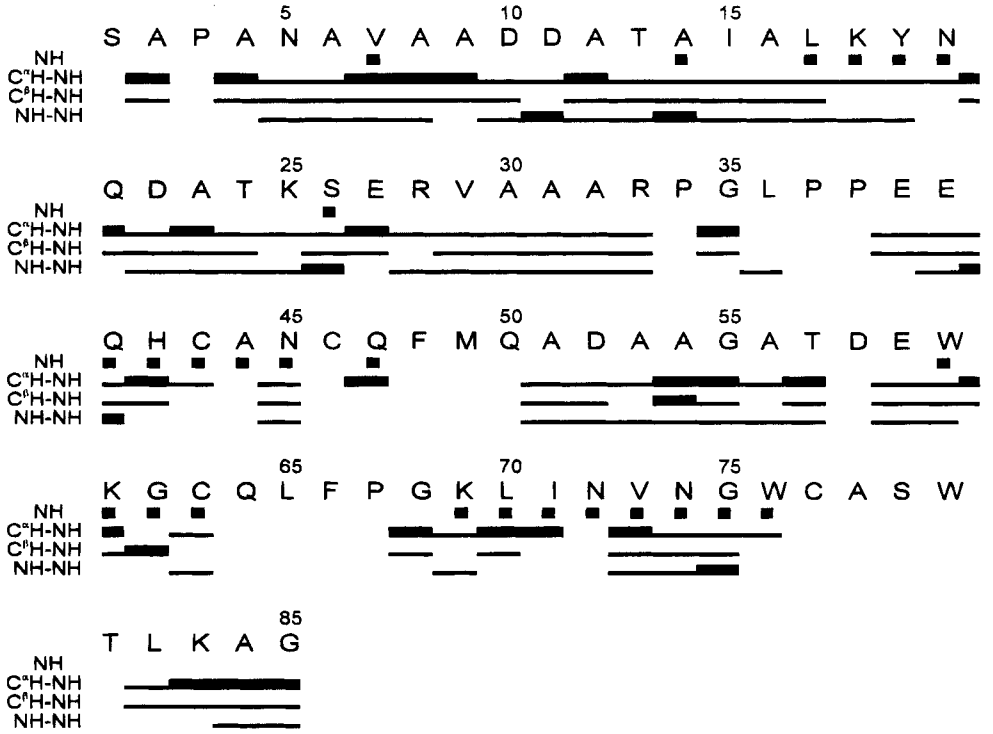

FIGURE 1: Schematic representation of the sequential connectivities involving NH, Hα, and Hβ protons in the oxidized HiPIP from *C. vinosum* obtained through standard 2D experiments. Dipolar NH−Hα connectivities are divided into strong (thick lines) and weak (thin lines). Filled squares indicate slowly exchanging NH protons.

restrained energy minimization (REM) and restrained molecular dynamics (RMD) calculations (Pearlman et al., 1991) on the 15 structures with the lowest target function values belonging to the distance geometry (DG) family (Güntert et al., 1991). For the iron and sulfur atoms and for the iron-bound cysteines, previously reported force field parameters were used (Banci et al., 1992). In a set of calculations made for comparison purposes, the charges of the eight cluster atoms were also uniformly increased by 0.125 to simulate reduction of the cluster (Banci et al., 1992).

The mean structure of the RMD family was subjected to further RMD calculations by including a 10 Å thick shell of water molecules. The trajectory was calculated for 216 ps, and the last 144 ps was used for structure averaging.

The analysis of NMR spectra as well as all DG, REM, and RMD calculations (double precision accuracy) were performed on IBM RISC 6000/530 computers.

RESULTS AND DISCUSSION

^1H and ^{15}N Assignment. An extensive assignment of the proton resonances of the oxidized HiPIP has already been published (Nettesheim et al., 1992). However, additional assignments were necessary in order to obtain the three-dimensional solution structure with a resolution similar to that of the reduced species (Banci et al., 1995). The available assignment of the ^1H and ^{15}N nuclei in the reduced protein is of great help for the assignment in the oxidized case.

Most of the spin systems were identified from 2D TOCSY experiments recorded with mixing time of 70 ms in water solution. Some spin systems were recognized from analogous experiments carried out in D_2O to detect CHα protons accidentally degenerate with water proton resonances. In total, 69 spin systems were identified from these experiments.

The sequence-specific assignment was performed following the method developed by Wüthrich and others (Wüthrich, 1986; Arseniev et al., 1988; Schultze et al., 1988). The comparative analysis of 2D NOESY and TOCSY maps allowed us to detect sequential connectivities (Figure 1) of 75 amino acids (Ser-1−Ala-2, Pro-3−Arg-33, Pro-34−Leu-36, Pro-38−Cys-43, Ala-44−Asn-45, Cys-46−Gln-47, Gln-50−Thr-57, Asp-58−Cys-63, Pro-67−Ile-71, Asn-72−Trp-76, and Thr-81−Gly-85). As in the case of the reduced protein, the largest continuous segment sequence-specifically assigned spans from Pro-3 to Arg-33, a protein region far from the cluster.

Out of 69 amino acids with identified spin patterns, 66 were also sequentially assigned. Two out of three Trp residues have been sequence-specifically assigned. The third tryptophan spin system can be assigned by exclusion to Trp-80. This assignment has been confirmed by many dipolar connectivities. The only A_3X system left can be assigned unambiguously as Ala-78. Further assignments were achieved through interresidual connectivities involving already assigned protons and by analogy with the connectivities found for the reduced protein.

The identification of the spin patterns of the cysteines and their sequence-specific assignment were obtained by 1D NOE experiments (Bertini et al., 1992). The NMR signals of all cysteine β-CH_2 protons are spread out of the diamagnetic spectral region and, therefore, allowed us to detect many connectivities. In the reduce case only some signals of the cysteine protons are outside the diamagnetic region.

In summary, 84 out of 85 amino acids were completely or partially assigned; only Ser-79 remained unassigned. A total of 417 protons were assigned, which correspond to 85% of all protons. It seems that, despite the increased paramagnetism, we were able to assign almost the same number of

protons as in the reduced case. Besides 154 proton resonances and 17 residues additionally assigned, the assignment agrees with that previously reported by Nettesheim et al. (1992).

The assignment of the ^{15}N resonances was achieved by comparison of the 2D $^{1}H-^{15}N$ HMQC spectra of the reduced and oxidized proteins. In total, 80% of all nitrogens were assigned for the oxidized protein, which compares with 90% of nitrogens assigned in the case of the reduced protein. While we could assign virtually the same number of protons for both oxidation states, the number of assigned nitrogens for the oxidized protein is smaller. The ^{1}H and ^{15}N NMR assignment of the oxidized HiPIP from *C. vinosum* is given as supplementary information.

Comments on Relaxation Rates and Chemical Shifts. Oxidized HiPIPs contain two Fe^{3+} and two $Fe^{2.5+}$ ions, all of them antiferromagnetically coupled one another. The resulting ground state is $S = {}^{1}/_{2}$ (Middleton et al., 1980). In the reduced state all iron ions are equivalent and $S = 0$ (Middleton et al., 1980). Therefore, oxidized HiPIPs are more paramagnetic than the reduced proteins, and consistently the hyperfine shifts of the protons of the coordinated cysteines are larger in the former case than in the latter (Phillips et al., 1974; Bertini et al., 1992). Despite that, the nuclear T_1s are longer for the more paramagnetic oxidized protein presumably because the electron relaxation rates are different.

The integration of the NOESY cross peaks should in principle be evaluated by taking into account the different nuclear T_1s of the protons giving rise to the cross peaks. This aspect, which is now under detailed investigation in our lab, has no practical effect on the quality of the structure, because (i) these cross peaks are translated into slightly larger upper distance limits, and (ii) they are few with respect to the whole body of constraints.

As far as the chemical shifts are concerned, most of them are the same as in the reduced species. In Figure 2A, the differences in proton chemical shifts per residue in the two redox forms are reported. The α-CH and β-CH_2 signals of coordinated cysteines are not taken into consideration. It appears that several backbone NH and Hα nuclei experience sizeable differences in the shifts (signals 1−10 in Figure 2A). It is reasonable to assume that, besides the NH experiencing hydrogen bonds with the sulfur atoms involved in coordination bonds with the iron ions (Phe-48, Leu-65, Cys-77, Ser-79, and Thr-81) (Backes et al., 1991) and those of the coordinated cysteines, the contact shift is zero. Pseudocontact shifts (PCS) might be important. However, the tetrahedral coordination around the metal ions should quench them (Bertini & Luchinat, 1986). Furthermore Fe(III) with ^{6}S ground state and little zero field splitting (ZFS) should not give rise to appreciable PCS. Only in heme containing system PCS have been measured, where the tetragonal distortion is large (La Mar et al., 1973; La Mar & Walker, 1979). Finally, besides an angular dependence, the PCS should decrease with the third power of the distance from the metal ions. Now, the differences in chemical shift for NH and Hα of Gln-47 have different signs, whereas their distance from the cluster is comparable. The same holds for Hα1 Gly-75 and NH Trp-76, NH and Hγ2 of Lys-69, and NH and Hα of Leu-82. Furthermore, protons at different distances but with their proton−proton vector pointing toward the cluster are found with opposite differences in

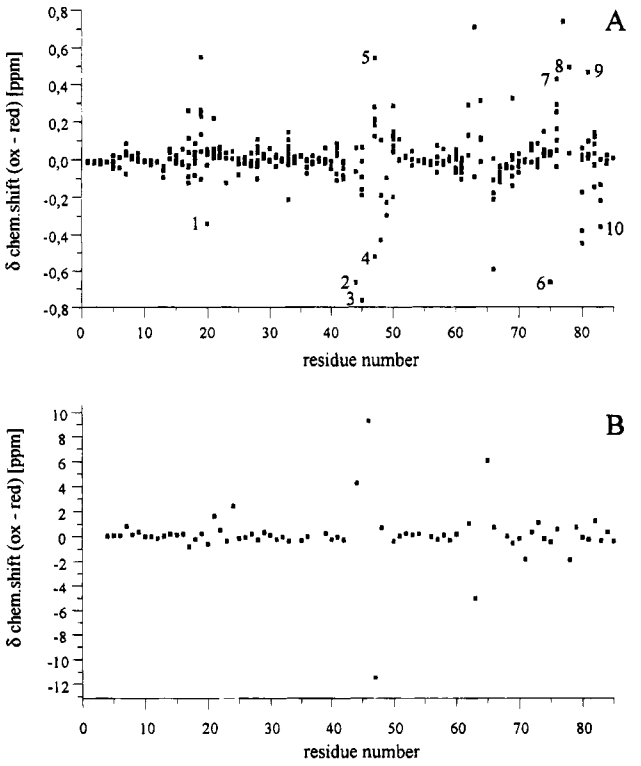

FIGURE 2: Differences in chemical shifts of the assigned ^{1}H (panel A) and ^{15}N (panel B) nuclei on passing from the oxidized to the reduced form in the HiPIP from *C. vinosum*. The resonances denoted by numbers belong to the following nuclei: 1, NH Asn-20; 2, Hα Ala-44; 3, NH Asn-45; 4, NH Gln-47; 5, Hα Gln-47; 6, Hα1 Gly-75; 7, NH Trp-76; 8, Hα Ala-78; 9, Hα Thr-81; 10, NH Lys-83.

chemical shifts, like NH/Hα of Gln-50 and Hγ2 of Lys-69/Hβ3 of Phe-66. Therefore, we conclude that PCS are not the major source of differences in chemical shifts between the oxidized and reduced forms of the protein. Such differences in shifts should then reflect structural changes which may eventually become significant when a higher degree of resolution of the structure will be available. The chemical shifts of ^{15}N (Figure 2B) are different only for NH groups either of coordinated cysteines (46, 63) or of immediately following residues (Ala-44, Gln-47).

Structure Determination. A total of 1498 constraints were obtained after running the CALIBA program (Güntert et al., 1991). Thirty-nine additional connectivities were added from 1D NOE difference spectra obtained by saturating the hyperfine shifted cysteine signals. The number of constraints constituting the upper distance limits, together with the corresponding values for the reduced protein, are presented in Table 1. The number of obtained constraints is similar for both oxidation states.

As in the case of the reduced protein, the three dimensional structure of the oxidized HiPIP from *C. vinosum* has been derived in three steps: distance geometry calculation (DG) using the program DIANA (Güntert et al., 1991), restrained energy minimization (REM), and restrained molecular dynamics (RMD) using AMBER 4.0 program package (Pearlman et al., 1991). During all calculations distance constraints have been applied. Out of 1537 distance constraints, 1142 have been taken into account by DIANA and consequently by REM and RMD calculations. All the used NOEs are primary, although the intensities may be affected by spin

Table 1: Number of NOE Constraints Constituting the Upper Distance Limits Files for the Reduced and Oxidized HiPIP from *C. vinosum*

class	definition	number of peaks (methyl peaks) reduced	number of peaks (methyl peaks) oxidized
1	intraresidue (except NH, Hα, Hβ)	344 (59)	370 (70)
2	sequential and intraresidue (NH, Hα, Hβ)	459 (62)	477 (67)
3	medium range	105 (14)	105 (14)
4	long range backbone	27	32
5	long range	554 (195)	553 (219)
total number of upper limits		1489	1537

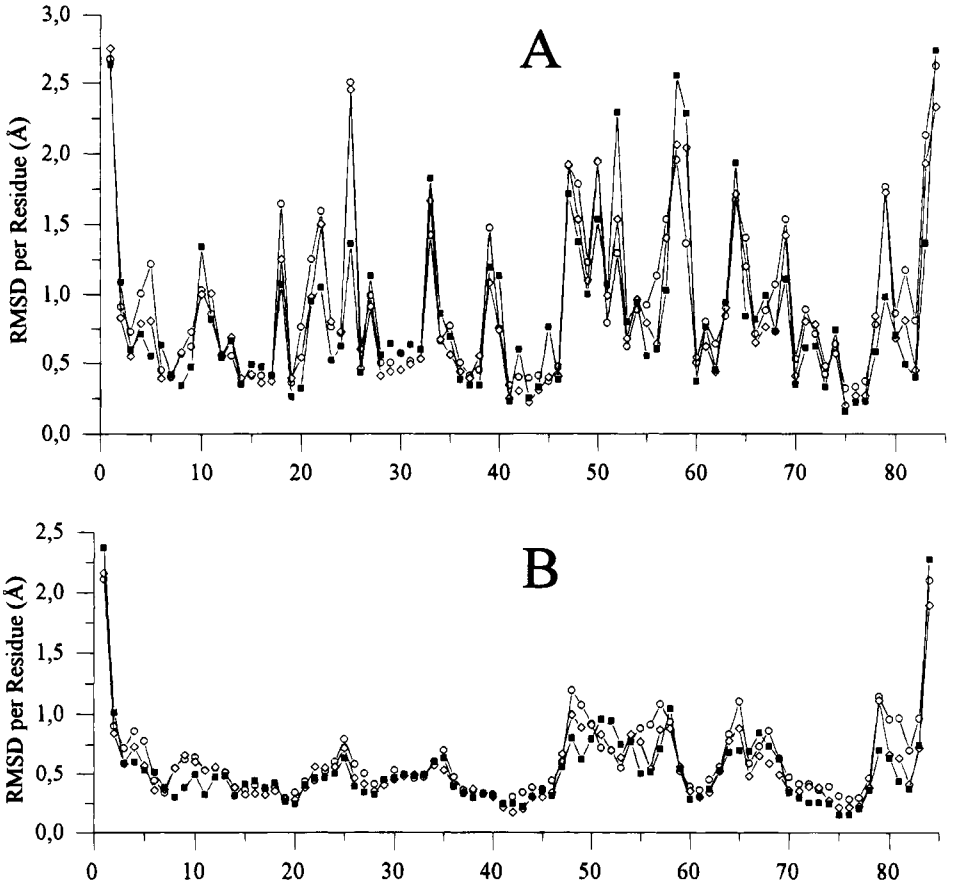

FIGURE 3: Diagrams of the RMSD per residue for the 15 accepted structures of the oxidized HiPIP from *C. vinosum* after DG (○), REM (◇) and RMD (■) calculations. RMSD values for the heavy atoms and the backbone are presented in panels A and B, respectively.

diffusion. Three hundred ninety-five constraints were found to be irrelevant for the structure determination.

A total of 658 DIANA structures were determined, interleaved by a total of 29 REDAC cycles (Güntert & Wüthrich, 1991), to generate redundant angle constraints. Fifty-six stereospecific assignments were obtained by using the program GLOMSA (Güntert et al., 1991).

Again in analogy with the reduced protein, the DG family consisted of 15 structures produced by DIANA with the lowest target function (<0.65 Å^2) and residual violation of distance constraints not exceeding 0.2 Å. The distribution of the RMSD per residue inside the DG family for both backbone and heavy atoms is shown in Figure 3. The average values of the RMSD within the DG family are 0.67 ± 0.09 and 1.09 ± 0.10 Å for backbone and heavy atoms, respectively. Comparing the DG family in both oxidation states, it seems that the quality and average RMSD values (Table 2) of these families are similar, the oxidized protein having slightly smaller RMSD values. This is due to the larger number of dipolar connectivities for the Phe-48 and Leu-65 containing regions which were poorly defined in the reduced case.

The REM family is characterized by average RMSD values of 0.59 ± 0.09 and 1.06 ± 0.09 Å, which are substantially decreased with respect to the DG family. The distribution of the RMSD per residue for the REM family is shown in Figure 3. The average RMSD values for the REM family are smaller than the corresponding values for both the REM and RMD families of the reduced protein (Table 2). Finally, the REM family was used as input for RMD calculations. The RMSD values for this family are 0.57 ± 0.14 and 1.08 ± 0.16 Å for the backbone and heavy atoms, respectively. No further improvement is observed on passing from the REM to the RMD family. The RMSD values for the RMD family of the oxidized proteins are lower than the corresponding values of the reduced protein by 0.05 and 0.11 Å, for the backbone and heavy atoms, respectively. The values of the target function for all three families together

Table 2: Average RMSD Values for Backbone (BB) and for All Heavy Atoms (HA) for the DG, REM, and RMD Families[a]

		DG	REM	RMD	RMDw
RMSD for residues Ala-2−Leu-82 (Å)	BB	0.67 ± 0.09	0.59 ± 0.09	0.57 ± 0.14	
	HA	1.09 ± 0.10	1.06 ± 0.09	1.08 ± 0.16	
target function (Å^2)		0.51			
target function (kJ mol^{-1})			58.46	70.84	75.91
total energy (kJ mol^{-1})			−5660.0	-7214.0	-6609.0
deviation from ideal bond distances (Å)					0.007
deviation from ideal bond angles (deg)					1.61

[a] For the last two families the average energy values are also reported. RMDw refers to the restrained energy minimized time-average of long RMD run in water.

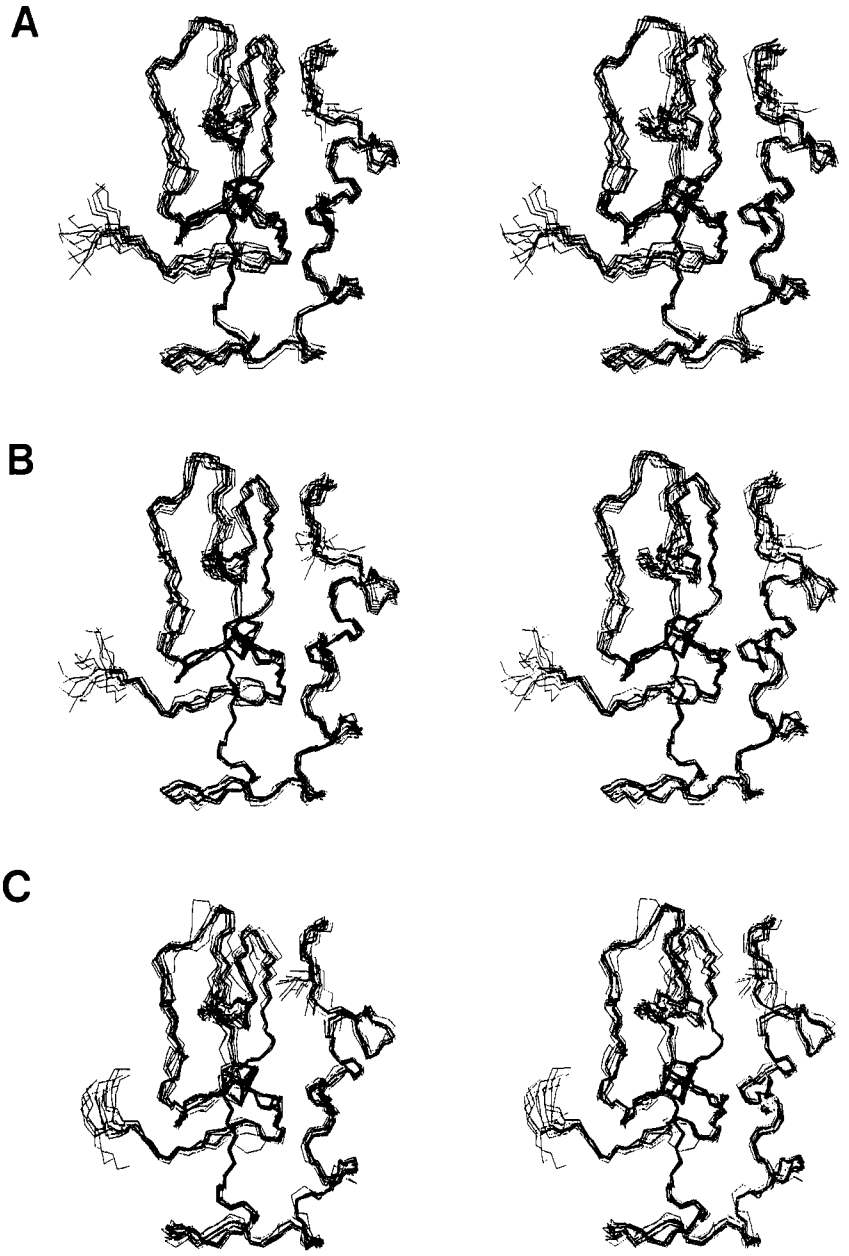

FIGURE 4: Stereodrawings of the 15 accepted structures of the oxidized HiPIP from *C. vinosum* obtained after DG (A), REM (B), and RMD (C) calculations.

with the conformational energies for the REM and RMD families are reported in Table 2.

The stereodrawings of the backbones of the DG, REM, and RMD families are presented in Figure 4. The conformations of the DG, REM, and RMD families are very close one to the other. The increase in resolution on passing from the DG to RMD family is apparent from the figure. However, RMD provides backbone conformations which deviate from the majority of conformations at some positions (Asp-52, Ala-54, Ser-79) (Figure 4), while still satisfying both distance and energy requirements.

The overall good quality of the structure is also confirmed by the order parameters (S) for the ψ and χ_1 dihedral angles (Hyberts et al., 1992). The S values for the backbone atoms

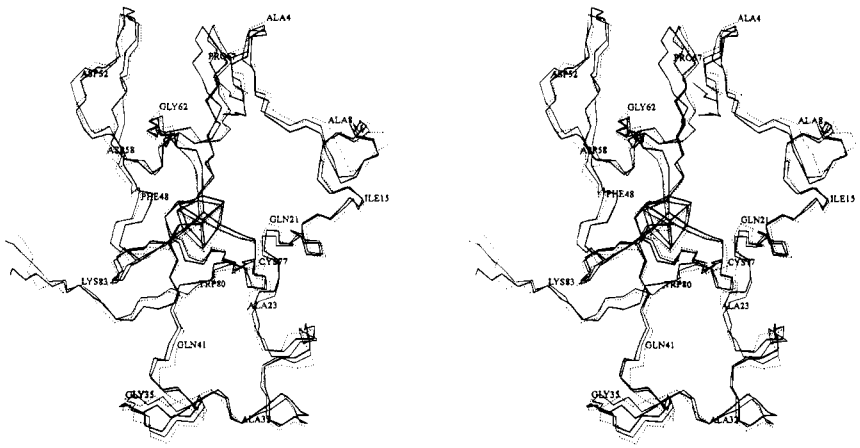

FIGURE 5: Stereodrawings of the backbone atoms of the solution structures of the oxidized (thick line) and reduced (thin line) forms and the X-ray structure (dotted line) of the oxidized HiPIP from *C. vinosum*.

of the N-terminal part of the protein are all very close to unity, thus indicating high order. S values sizably smaller than unity are only observed for ψ of residues Gln-47, Gln-50, Cys-63, and Trp-80 and for χ_1 of residues Asp-52, Asp-58, and Glu-59.

The mean structure of the RMD family was subjected to further RMD calculations in water. In the structure obtained in this way (RMDw) the interaction of water with the protein is taken into account. The RMDw structure is in good agreement with the RMD family and thus can be considered as a further refinement of the RMD family. Energies and target functions of the RMDw structure together with the values of the root mean square deviations of bonds (0.007 Å) and angles (1.61°) from ideal values are reported in Table 2. All the ϕ and ψ dihedral angles fall within the allowed Ramachandran regions. This indicates that the backbone has an overall allowed low-energy conformation.

Comparison of the Structures of the Reduced and Oxidized Proteins. As the solution structure of the reduced (Banci et al., 1995) as well as the solid state structure of the oxidized HiPIP (Carter et al., 1974) from *C. vinosum* are available, we will try to figure out whether differences occur in the structures while either changing the oxidation state or passing from solid state to solution. The backbones of the solution structures together with the backbone of the solid-state structure of the oxidized protein (the latter called the solid-state structure hereafter) are shown in Figure 5. Overall, these structures exhibit a high degree of analogy. Actually, this result is expected when taking into consideration that electron transfer proteins have quite rigid structures. Therefore, they might not experience dramatic changes while going from one oxidation state to the other. However, less prominent structural changes upon oxidation (reduction) may occur, and their elucidation can be important for the understanding of the electron transfer processes. A very recent report is available which compares a reduced cysteine containing protein with the oxidized form containing a disulfide bridge. Only subtle conformational changes occur upon changing redox state (Jeng et al., 1994).

By comparing the RMDw structures for the oxidized ($RMDw_{ox}$) and reduced ($RMDw_{red}$) forms (Table 3), we find that the average RMSD values for the backbone and heavy atoms are 0.65 and 1.14 Å, respectively. RMSD values of 0.76 and 1.25 Å for the backbone and heavy atoms, respectively, are observed between $RMDw_{ox}$ and X-ray structure, and values of 0.61 and 1.19 Å between $RMDw_{red}$ and the X-ray structure. These RMSD values between the two forms are slightly larger than the RMSD values within the RMD families of the present oxidized and reduced (Banci et al., 1995) solution structures and therefore may reflect modest but real structural differences between the three forms.

Table 3: Pairwise Comparison (RMSD Values for the Backbone and Heavy Atoms) of the Structures Obtained during the Calculations of the Solution Structures of the Oxidized and Reduced HiPIP from *C. vinosum*

	$RMDw_{ox}$ (Å)	$RMDw_{red}$ (Å)	o (Å)[a]	r (Å)[a]	X-ray (Å)	
$RMDw_{ox}$	0.57[b]	0.65	0.49	0.66	0.76	BB
	1.08	1.14	0.98	1.11	1.25	HA
$RMDw_{red}$		0.62[c]	0.77	0.47	0.61	BB
		1.19	1.30	1.13	1.19	HA
o				0.71	0.78	BB
				1.01	1.25	HA
r					0.51	BB
					0.97	HA

[a] RMDw structures obtained by starting from the X-ray structure and using only those NOE constraints in common to both oxidized (o) and reduced (r) solution data. [b] Within the RMD family for the oxidized protein. [c] Within the RMD family for the reduced protein.

The distributions of the RMSD for the backbone atoms relative to (i) solution structures, (ii) the solution structure of the oxidized protein and the solid-state structure, and (iii) the solution structure of the reduced protein and the solid state structure are shown in Figure 6. Analyzing these data, it can be observed that the three structures coincide well in the region Asp-11−Asn-20 and Leu-70−Trp-80. For the remaining regions the solution structure of the reduced protein is closer to the solid-state structure (which is that of the oxidized protein) than the solution structure of the present oxidized species, as already noticed from the overall RMSD values. Although possibly premature at this stage, the possibility could be considered that X-ray irradiation reduces, at least partially, the protein (see, however, later).

For pairwise comparison between the two solution structures, between the $RMDw_{ox}$ and the solid state structure, and between the $RMDw_{red}$ and the solid-state structure in terms of dihedral angles, we have used the S values for the ψ and χ_1 dihedral angles. The deviations are fewer than expected from the RMSD values; we also observe that the ψ backbone dihedral angles inside each pair are much more similar than

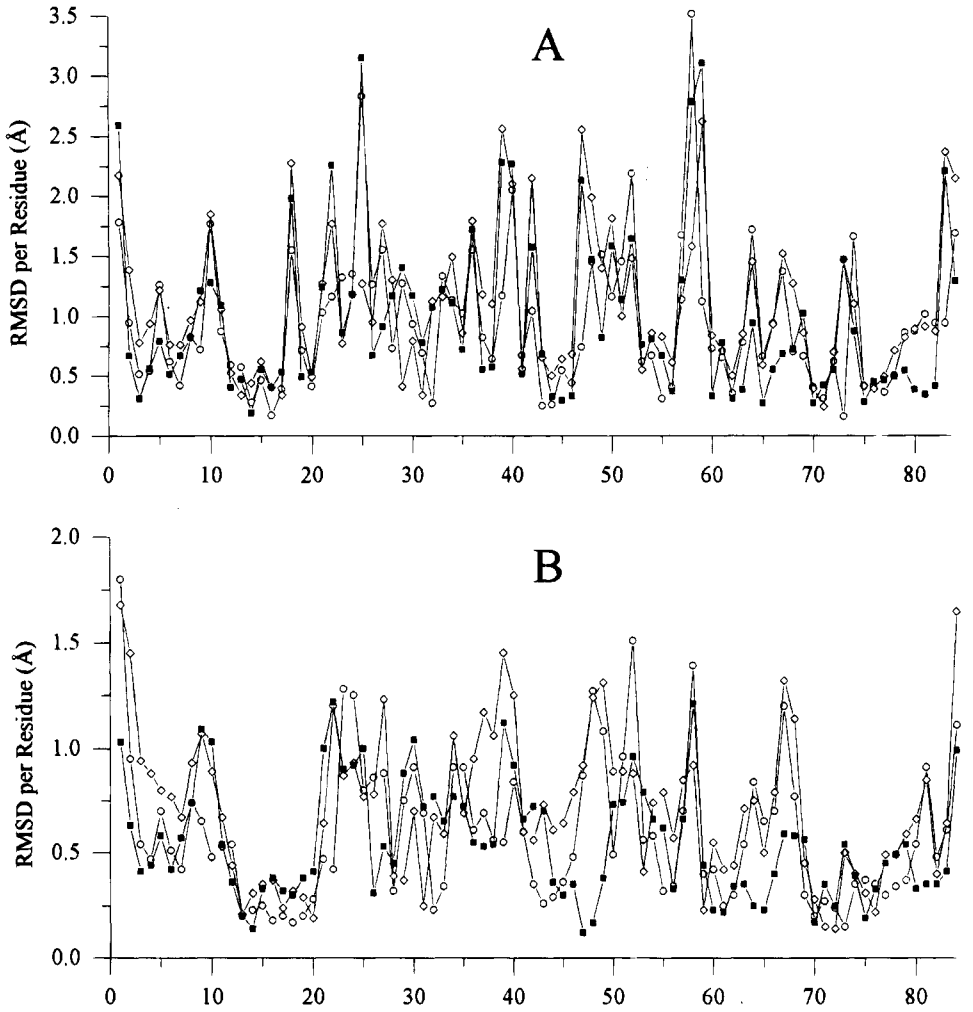

FIGURE 6: Diagrams of the pairwise RMSD per residue for the backbone (B) and heavy atoms (A) of the RMDw structures of the reduced and oxidized proteins (○), X-ray structure of the oxidized protein and the RMDw structure of the reduced protein (■), and X-ray structure of the oxidized protein and the RMDw structure of the oxidized protein (◇).

the corresponding χ_1 side chain dihedral angles, as expected.

By analyzing the backbones of the two solution structures, we note that while in terms of the local RMSD values some amino acids show large deviations (Figure 6) (Ala-23, Thr-24, Ser-26, Glu-27, Ala-30, Pro-34, Gly-35, Glu-40, Met-49, Asp-58, Gln-64, Pro-67, and Thr-81), almost complete identity of the two structures in terms of S values for the ψ dihedral angles occurs. Therefore, the large values of the RMSD for the backbone atoms observed when comparing the two solution structures arise mainly from translations of parts of the backbones, but not from real changes of conformation. At the same time, the differences in the backbone atom RMSD values for the residues Lys-25, Phe-48, Ala-51, and Asp-52 are also maintained in the ψ dihedral angles. This implies that some differences can really be present at these positions. We also observe that two amino acids (Ser-79 and Trp-80) are quite similar in terms of RMSD for backbone atoms while they show substantial differences between the corresponding ψ dihedral angles. The scarcity of constraints for the backbone atoms of these two residues does not allow us to draw definite conclusions.

By comparing each solution structure with the solid-state structure considering the S values for the ψ dihedral angles, we also observe close correspondence between the solution structures and the solid-state structure. Again we note that $RMDw_{red}$ is more similar to the X-ray structure than $RMDw_{ox}$ also in terms of S values.

The S values for the χ_1 side chain dihedral angles obtained when comparing the two solution structures are sizably lower than unity for the following amino acids: Asp-10, Lys-25, Arg-28, Asp-52, Thr-57, Asp-58, and Gln-64. Apart from Arg-28, all these amino acids are characterized also by high values of the RMSD for heavy atoms while comparing the $RMDw_{ox}$ and $RMDw_{red}$ structures, and, therefore, their position can actually differ in the oxidized and reduced forms.

A slight movement of the cluster is also apparent by comparing the RMDw structures of the reduced and oxidized forms. The cluster in the oxidized form can be described as being slightly shrinked and slightly more buried inside the protein. The movement is roughly along the Fe−Cys-43 bond direction, the iron atom bound to Cys-43 and the Cys-43 sulfur moving by about 0.2 Å toward the interior of the protein, and the sulfide ion opposite to the above iron ion moving inward by about 0.6 Å. The other three iron ions and the relative cysteine sulfurs and sulfide ions accompany this movement (Figure 5).

In an attempt to establish whether some of the differences between the reduced and oxidized structures were due to the different cluster charges, an RMD_w run was performed using the constraints of the oxidized species but with cluster charges of the reduced form. The resulting structure was

almost superimposable to that obtained with the cluster charges of the oxidized protein. This shows that indeed the NOE constraints by themselves ensure two different families for the oxidized and reduced proteins, as it appears also from the direct comparison of the DG structures. As a further check, we have selected the X-ray structure of the oxidized *C. vinosum* as an independent starting structure and subjected it to two RMD runs in water, applying only those NOE constraints for the reduced and oxidized forms which were detected in both cases, thus obtaining two structural models which we termed "o" (with constraints for the oxidized protein) and "r" (with constraints for the reduced protein). This has been performed to observe how the same constraints, obviously with different intensities, influence the structure calculations. The results are shown in Table 3. It appears that a clearcut discrimination between the two structures is achieved.

From the above analysis it appears that some differences between the solution structures and between the solution structures and the solid-state structure indeed exist. However, the resolution of both the X-ray and solution structures may be not high enough to allow us to identify specific small structural changes.

Concluding Remarks. The solution structure of the oxidized HiPIP from *C. vinosum* is solved at a satisfactory degree of resolution, especially if the paramagnetism of the protein is taken into consideration. The structure shows subtle conformational differences from that of the reduced protein, which was solved earlier. The RMSD between the two families points out that we are in the presence of two different structures, but every single variation should be considered with caution in the absence of a further structural refinement. Both oxidized and reduced structures are similar to the X-ray structure, although the RMSD values indicate a larger similarity of the latter with the reduced protein.

We have also shown that, by starting from the X-ray structure and by using the NMR constraints available for both oxidized and reduced proteins, two different structures are generated which are reasonably similar to those independently obtained as solution structures.

At any rate, we consider most of the differences at the borderline of our present resolution, and any speculation on its possible significance in relation to cluster reorganization energy should await further experimental confirmation.

ACKNOWLEDGMENT

A.D. thanks the International Centre for Genetic Engineering and Biotechnology and D.H.W.K. thanks the C. E. C. Human Capital and Mobility Program for research postdoctoral fellowships. P.S. thanks the Italian Ministry of Foreign Affairs for a Ph.D. grant.

SUPPORTING INFORMATION AVAILABLE

Listing of 1142 experimental NOE and NOESY intensities used for the structure calculation and the ^{15}N and ^{1}H NMR assignments of the oxidized HiPIP from *C. vinosum* (20 pages). Ordering information is given on any current masthead page.

REFERENCES

Arseniev, A., Schultze, P., Worgotter, E., Braun, W., Wagner, G., Vasak, M., Kagi, J. H., & Wüthrich, K. (1988) *J. Mol. Biol. 201*, 637−657.

Backes, G., Mino, Y., Loehr, T. M., Meyer, T. E., Cusanovich, M. A., Sweeney, W. V., Adman, E. T., & Sanders-Loehr, J. (1991) *J. Am. Chem. Soc. 113*, 2055−2064.

Banci, L., Bertini, I., & Luchinat, C. (1991) *Nuclear and Electron Relaxation. The Magnetic Nucleus-Unpaired Electron Coupling in Solution*, VCH, Weinheim.

Banci, L., Bertini, I., Carloni, P., Luchinat, C., & Orioli P. L. (1992) *J. Am. Chem. Soc. 114*, 10683−10689.

Banci, L., Bertini, I., Eltis, L. D., Felli, I. C., Kastrau, D. H. W., Luchinat, C., Piccioli, M., Pierattelli, R., & Smith, M. (1994) *Eur. J. Biochem. 225*, 715−725.

Banci, L., Bertini, I., Dikiy, A., Kastrau, D. H. W., Luchinat, C., & Sompornpisut, P. (1995) *Biochemistry 34*, 206−219.

Bartsch, R. G. (1978) *Methods Enzymol. 53*, 329.

Bertini, I., & Luchinat, C. (1986) *NMR of Paramagnetic Molecules in Biological Systems*, Benjamin/Cummings, Menlo Park, CA.

Bertini, I., Briganti, F., Luchinat, C., Scozzafava, A., & Sola, M. (1991) *J. Am. Chem. Soc. 113*, 1237−1245.

Bertini, I., Capozzi, F., Ciurli, S., Luchinat, C., Messori, L., & Piccioli, M. (1992) *J. Am. Chem. Soc. 114*, 3332−3340.

Breiter, D. R., Meyer, T. E., Rayment, I., & Holden, H. M. (1991) *J. Biol. Chem. 266*, 18660−18667.

Carter, C. W. J., Kraut, J., Freer, S. T., Xuong, N.-H., Alden, R. A., & Bartsch, R. G. (1974) *J. Biol. Chem. 249*, 4212−4215.

Clore, G. M., & Gronenborn, A. M. (1994) *Protein Sci. 3*, 372−390.

Dus, K., DeKlerk, H., Sletten, K., & Bartsch, R. G. (1967) *Biochim. Biophys. Acta 140*, 291−311.

Güntert, P., & Wüthrich, K. (1991) *J. Biomol. NMR 1*, 447−456.

Güntert, P., Braun, W., & Wüthrich, K. (1991) *J. Mol. Biol. 217*, 517−530.

Hyberts, S. G., Goldberg, M. S., Havel, T. F., & Wagner, G. (1992) *Protein Sci. 1-I*, 736−751.

Jeng, M-F., Campbell, A. P., Begley, T., Holmgren, A., Case, D. A., Wright, P. E., & Dyson, H. J. (1994) *Structure 2*, 853−868.

La Mar, G. N., Ed., (1995) *NMR of Paramagnetic Macromolecules. NATO ASI Series* Kluwer Academic, Dordrecht.

La Mar, G. N., & Walker, F. A. (1979) in *The Porphyrins* (Dolphin, D., Ed.) pp 61−157, Academic Press, New York.

La Mar, G. N., Eaton, G. R., Holm, R. H., & Walker, F. A. (1973) *J. Am. Chem. Soc. 95*, 63−75.

Luchinat, C., & Ciurli, S. (1993) *Biol. Magn. Reson. 12*, 357−420.

Middleton, P., Dickson, D. P. E., Johnson, C. E., & Rush, J. D. (1980) *Eur. J. Biochem. 104*, 289−296.

Moss, T. H., Petering, D., & Palmer, G. (1969) *J. Biol. Chem. 244*, 2275−2277.

Nettesheim, D. G., Harder, S. R., Feinberg, B. A., & Otvos, J. D. (1992) *Biochemistry 31*, 1234−1244.

Pearlman, D. A., Case, D. A., Caldwell J. C., Siebel, G. L., Singh, U. C., Weiner, P., & Kollman, P. A. (1991) in *AMBER 4.0*, University of California, San Francisco.

Phillips, W. D., McDonald, C. C., Stombaugh, N. A., & Orme-Johnson, W. H. (1974) *Proc. Natl. Acad. Sci. U.S.A. 71*, 140−143.

Pochapsky, T. C., Mei Ye, X., Ratnaswamy, G., & Lyons, T. A. (1994) *Biochemistry 33*, 6424−6432.

Schultze, P., Worgotter, E., Braun, W., Wagner, G., Vasak, M., Kagi, J. H., & Wüthrich, K. (1988) *J. Mol. Biol. 203*, 251.

Wüthrich, K. (1986) *NMR of Proteins and Nucleic Acids*, Wiley, New York.

BI950640S